Journal of Applied Mechanical Engineering
ISSN: 2168-9873

Kouadri et al., J Appl Mech Eng 2017, 6:3
DOI: 10.4172/2168-9873.1000269

Research Article Open Access

Experimental and Theoretical Analysis of the Chip Flow Direction in Turning using Flatted and Grooved Inserts – Impact of the Tool Rake Face Geometry, the Work Material and Cutting Conditions

Kouadri S[1]*, Bensari A[2] and Tirenifi M[2]

[1]Superior School of Material, BP 188 Beau-lieu, Algiers, Algeria
[2]University of Mascara, BP 29 Route de Mascara , Mascara, Algeria

Abstract

This paper deals mainly with an experimental and theoretical analysis of the Chip Flow Direction (CFD) in turning process using flatted and grooved inserts. Turning tests have been performed to determine the CFD from measured cutting force components. Different cutting conditions have been considered by varying the cutting speed, the feed rate and the depth of cut. From a theoretical point of view, two models have been applied. The first one is an analytical model based on the discretization of the undeformed chip area. The second one is a purely geometrical model which assumes the CFD normal to the major axis of the projected cutting area on the rake face. The effect of cutting conditions on the CFD was clearly highlighted experimentally and by adopted models. It has been shown that the CFD depends strongly on the depth of cut in the browsed range of cutting parameters, while cutting speed has a little effect. One of main discussed results concerns the impact of the tool rake face geometry (flatted and grooved) on the CFD. Finally, it has been shown that the CFD is independent on machined materials.

Keywords: Turning; Chip flow direction; Cutting force; Tool geometry; Grooved insert; Cutting condition

Nomenclature

V_c Cutting speed

f Feed rate

d Depth of cut

d' Projected depth of cut on the rake face plane

r Tool nose radius

K_r Approach angle

C_e End cutting edge angle

C_s Side cutting edge angle

C_s' Projected angle of Cs on rake face plane

i Inclination angle of tool

α_n Normal rake angle

P_r, P_p, P_f, P_n, P_s, P_s' Planes used for the definition of tool angles

F_c, F_f, F_p Force components (cutting, feed and depth of cut forces)

F_0 Friction force at tool-chip interface

dF_0, dF_{0x}, dF_{0y} Friction force acting on a chip element and its components

F_0, F_{0x}, F_{0y}, Resultant of dF_0, dF_{0x} and dF_{0y}, respectively

u Friction force intensity

A, B, S Area of undeformed chip section

dA Area of undeformed section of chip element

ds Differential length of cutting edge

$t(s)$ Varying undeformed chip thickness

θ Angle made by positive X axis with the undeformed chip element

θ_0, θ_1, θ_2, θ_3, Limit angles of integration

Ω_0 Angle made by elemental undeformed chip or dF_0 with the positive Y axis

$\overline{\Omega}_o$ Angle made by the friction force F_0 with the positive Y axis

η_c Chip flow angle measured from the normal to the side cutting edge

COF Coefficient of friction

Introduction

The control of chips formation and chips flow in machining pro cesses are important to facilitate their evacuation and to avoid interaction during cutting between chips and the machined part. In such situation, chips may alter the workpiece surface quality if it is badly directed. Jared and Dow [1] stated that under some cutting conditions, contact between chips and the machined workpiece can result in superficial damage to the finished surface. Therefore, estimating the chip flow direction allows improving the machining operation by choosing adequate cutting conditions as well as geometrical characteristics of cutting tools. It is important to distinguish between the local chip flow direction, at the exit of the cutting zone (immediate vicinity of the active or engaged cutting edge), and the global chip flow direction (far from the cutting zone). The chip flow direction analysed in this work corresponds to the local one, and is frequently characterised by

***Corresponding author:** Kouadri S, Superior School of Material, BP 188 Beau-lieu, Algiers, Algeria, Tel: +213 (45) 804169; E-mail: kouadri.sofiane@yahoo.fr

Received April 17, 2017; **Accepted** June 02, 2017; **Published** June 06, 2017

Citation: Kouadri S, Bensari A, Tirenifi M (2017) Experimental and Theoretical Analysis of the Chip Flow Direction in Turning using Flatted and Grooved Inserts – Impact of the Tool Rake Face Geometry, the Work Material and Cutting Conditions. J Appl Mech Eng 6: 269. doi: 10.4172/2168-9873.1000269

the angle between the normal to the side (main) cutting edge and the direction of chip flow on rake face of the cutting tool.

To estimate the chip flow direction, several models are proposed in literature. The earliest model is attributed to Stabler [2], who was considered that in oblique cutting configuration the chip flow angle is equal to the inclination angle of the insert (i.e. $\eta_c = i$). This rule has been found to be only as a first approximation (Stabler [3]; Armarego and Brown, [4]. In later work, Stabler (1964) proposed another law by introducing a correction factor ($\eta_c = k.i$, with $0.9<k<1$). The parameter k depends on the workmaterial and cutting conditions; it is suggested that at low cutting speed, k approaches unity. Colwell [5] proposed a very simplified geometrical model which assumed the CFD normal to the major axis of the projected cutting area on the rake face. In case of nose radius inserts, this axis corresponds to the segment joining the extreme points of engaged cutting edge. Wang and Mathew [6] stated that the estimated CFD with Colwell's model satisfied only the case of zero tool inclination and rake angles (i.e. $i = \alpha_n = 0$). To take into account inclination and rake angles effects on the CFD, Russell and Brown [7] proposed an empirical law ($\eta_c = \tan^{-1}[\tan i \cos \alpha_n]$) and showed a good agreement with experimental data. Kronenberg [8] assumed later that the CFD was in the velocity rake face, and proposed the following relationship: ($\eta_c = \tan^{-1}[\tan i \sin \alpha_n]$. To take into account the effect of cutting speed, Zorev [9] proposed an empirical power law as a function of inclination angle and cutting speed ($\eta_c = iV_c^{-0.08}$). As it can be seen in the present study, the CFD depends weakly on the cutting speed compared to the effect of feed rate and depth of cut. All previous models did not take into account the machined and tool materials.

Physical models, which include workmaterial behaviour, were developed for oblique cutting configuration to predict the chip flow angle. For example, Moufki et al. [10] have been proposed a thermo-mechanical modelling to predict cutting forces, shear angle, cutting temperature as well as the orientation of the chip flow. Their approach was based on the discretization of the cutting edge and assumes a flat cutting face. As input data of the model, they use thermomechanical parameters of the tool and workpiece materials. Strenkowski et al. [11] proposed a combined analytical-numerical model, based on Usui's energy model (Usui et al., [12]; Usui and Hirota, [13]) for the analytical calculation and Eulerian finite element model for the numerical calculation. Usui's energy model is based on the minimisation of shear and friction energies to find the chip flow angle. The proposed hybrid model predicts well the CFD and cutting forces. Other models are proposed based on energy minimisation. Seethaler and Yellowley [14] have proposed a so called "Upper-bound model" based on the minimisation of the cutting power (sum of shear and friction energies) to predict chip flow angle. This approach was extended later by Adibi-Sedeh et al. [15] and recently improved by Zou et al. [16]. Fang [17] has developed a similar approach to determine the chip flow angle and also the chip flow speed.

Nowadays, in machining processes the major cutting inserts present a grooved (non-flatted) rake face. Hence to control the chip flow it is interest to know the CFD in such cases with respect to cutting parameters variation. For this purpose, two turning cases have been analysed; one with flatted rake face insert and the other with grooved rake face insert. Experimental tests have been performed with varying the cutting speed, the feed rate and the depth of cut, and the measurement of cutting force components for each cutting condition. For the analysis purpose, two models are considered: the Wang and Mathew analytical model Wang and Mathew [18] based on the discretization of undeformed chip area (considered as flat), and the Colwell model (Colwell, 1954), based on purely geometrical considerations. The predicted chip flow angles with these two models are compared to the experimental ones. The analysis highlights the effect of the rake face geometry and cutting parameters on the CFD, and gives an indication about the validity of assumptions of adopted models.

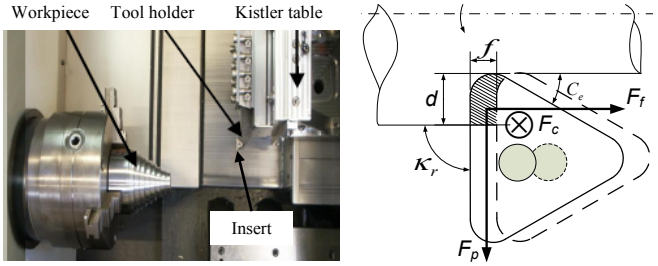

Figure 1: (a) Experimental setup and (b) definition of measured cutting force components and cutting configuration ($C_S = 0°$ or $K_r = 90°$, $C_e = 30°$, $i = 0°$, $\alpha_n = 0°$).

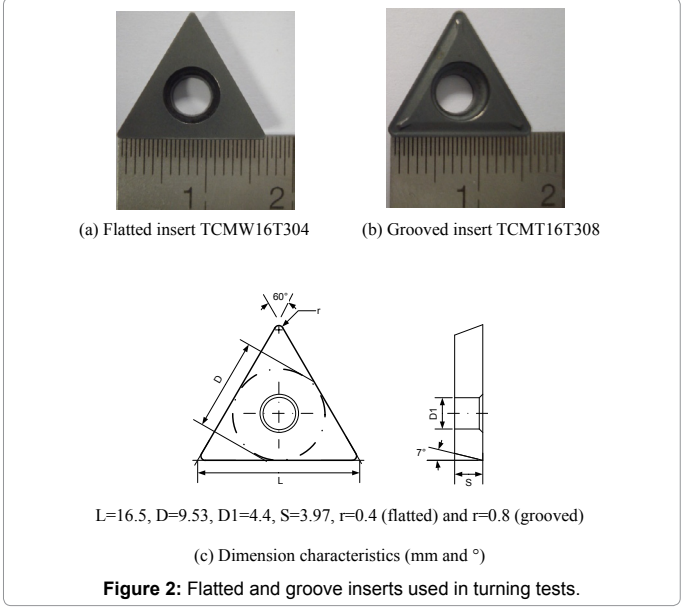

Figure 2: Flatted and groove inserts used in turning tests.

Experimental Work

Two separate turning tests have been performed, one using flatted inserts and the other using grooved inserts, to analyse the CFD. Cutting tests were performed on CNC lathe which allows the variation of cutting conditions in a large range. The machine is instrumented with a dynamometer system for the measurement of cutting force components (Fc, F_f and F_p). The machining device is shown in Figure 1(a), and the definition of measured cutting force components and cutting configuration is illustrated in Figure 1(b).

Uncoated triangular flatted inserts, designated by TCMW16T304 (Figure 2(a)), and AISI 1045 (a ferrite-perlite steel) as a workmaterial were chosen for the first turning tests. The selected cutting conditions are reported in Table 1. While coated triangular grooved inserts, designated by TCMT16T308 (Figure 2(b)), and AISI 304L as a workmaterial (a stainless steel) were chosen for the second turning tests. The selected cutting conditions are reported in Table 2. The browsed range of each cutting parameter, for the two cases, has been chosen from recommendations of tools manufacturers for considered tool/work material couples.

***f* = 0.1 mm/tr, *d* = 1.1 mm**												
50	100	150	180	200	250	300	350	400	450	500	600	700
***Vc* = 250 m/min, *d* = 1.1 mm**												
0.10		0.125	0.15		0.175		0.20	0.225	0.275		0.30	
***Vc* = 250 m/min, *f* = 0.26 mm/tr**												
0.70		0.80	0.90		1.00	1.10	1.20	1.30			1.40	

Table 1: Cutting conditions used for machining AISI 1045 with flatted insert TCMW16T304.

***f* = 0.2 mm/tr, *d* = 1 mm**								
20	50	100	150	200	250	300	400	500
***Vc* = 100 m/min, *d* = 1 mm**								
0.05	0.10		0.15	0.20	0.25	0.30		0.35
***Vc* = 100 m/min, *f* = 0.15 mm/tr**								
0.20	0.50		1.00	1.50	2.00	2.50		3.00

Table 2: Cutting conditions used for machining AISI 304L with grooved insert TCMT16T308, from Kagnaya.

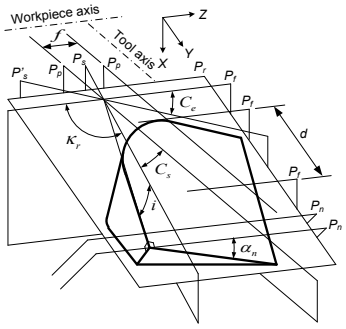

Figure 3: Definition of the main cutting angles for nose radius insert.

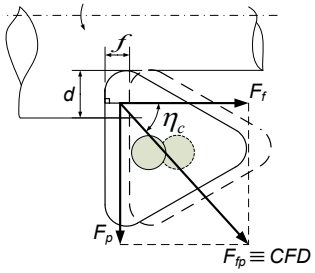

Figure 4: Definition of CFD from feed and depth of cut force components ($\alpha_n = i = 0$).

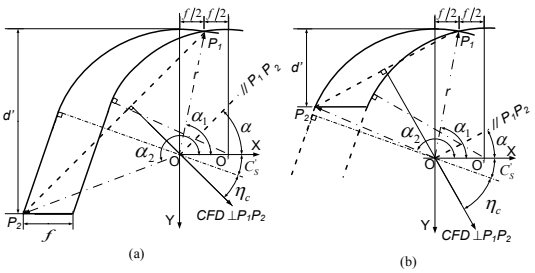

Figure 5: Geometric conditions of chip flow for a nose radius insert, based on geometrical Colwell model.

Assessment of the Chip Flow Direction

In order to analyse the CFD in turning with flatted and grooved inserts, two models were selected among those proposed in the literature: Colwell model (Colwell, 1954) and Wang and Mathew model (Wang and Mathew, 1995). Wang (2001) and Kishawya et al. [19] adopted later similar approach as Wang and Mathew. These models were chosen to account for the nose radius effect. Colwell model is purely geometrical while the Wang and Mathew model is developed under the assumption that the tool rake face is flat. This allows showing their ability to predict the CFD when machining with complex tool geometries, and therefore highlighting the effect of rake face geometry on the CFD. Figure 3 illustrates tool angles, defined on nose radius insert, used in analytical formulations described in following sections Figure 4.

CFD Deduced from Measured Cutting Force Components

To estimate the CFD from experimental data, the assumption that the CFD is collinear with the tangential (frictional) force applied on the rake face is made [20,21]. The same assumption was considered by Moufki et al. (2000) in their thermomechanical model. Although using experimental data, Yegneswaran [22] has shown that the CFD may slightly deviate from the frictional force direction. In considered cutting configuration ($\alpha_n = i = 0$), for both cases (machining with flatted and grooved inserts) the CFD corresponds to the direction of the resultant feed force and depth of cut components (i.e. $CFD // F_{fp}$). The obtained CFD is taken as the experimental flow direction, given for α_n=i=0 by the following relation:

$$\eta_c = \tan^{-1}(F_p / F_f) \backslash^* \quad (1)$$

CFD Predicted by the Geometrical Colwell Model

Colwell model is purely geometrical, assuming the CFD normal to the major axis of the projected area of cut on the rake face. In case of nose radius inserts, this axis corresponds to the segment joining the extreme points of the engaged cutting edge, as illustrated in Figure 5. Four cases can be defined, as reported e.g. by Wang and Mathew (1995). Here only two cases are considered, corresponding to the engagement of the main cutting edge and/or nose radius edge. It includes all undeformed chip areas obtained with cutting conditions of Table 1 and Table 2, used in experiments. The two other cases correspond in addition to the engagement of the end cutting edge.

Case 1: engaged side cutting and nose radius edges: $d' \geq r\left(1-\sin C_s'\right)$ and $f \leq 2r \sin Ce$

Where d' is the projection of depth of cut, d, in the rake face, given by

$$d' = d \cos C_s \sec i \left[\left(\tan\alpha_n \tan C_s + \sin i\right)^2 + \cos^2 i \sec^2 C_s\right]^{1/2} \quad (2)$$

To derive the chip flow angle, the slope of the segment $[P_1,P_2]$ is to define. First, the coordinates of points P_1 and P_2 (see **Fig. 5(a)**) are given by:

$$P_1\begin{cases} x_1 = r\cos\alpha_1 \\ y_1 = r\sin\alpha_1 \end{cases}, \qquad P_2\begin{cases} x_2 = r\cos^{-1}\alpha_1 + (d'-r)\tan\alpha_1 \\ y_2 = d'-r \end{cases} \quad (3)$$

With $\alpha_1 = \cos^{-1}(f/2r)$.

The slope of the segment $[P_1,P_2]$ can be defined by the angle between the X axis and this segment, given as

$$\alpha = \tan^{-1}\left(\frac{r(1+\sin\alpha_1) - d'}{r\cos\alpha_1 - r\cos^{-1}\alpha_1 - (d'-r)\tan\alpha_1}\right) \quad (4)$$

According to Colwell model, the CFD is the normal to this segment.

Thus chip flow angle is obtained by the relation

$$\eta_c = \pi/2 - C_s^{'} - \alpha \tag{5}$$

Case 2: engaged nose radius edge: $d' \le r\left(1-\sin C_s^{'}\right)$ and $f \le 2r \sin Ce$

For this case, coordinates of points P_1 and P_2 in **Figure 5(b)** are

$$P_1\begin{cases} x_1 = r\cos\alpha_1 \\ y_1 = r\sin\alpha_1 \end{cases}, \qquad P_2\begin{cases} x_2 = r\cos\alpha_3 \\ y_2 = r\sin\alpha_3 \end{cases} \tag{6}$$

With $\alpha_1 = \cos^{-1}(f/2r)$ and $\alpha_{3=}\ \pi\text{-}\sin^{-1}((r\text{-}d)/r)$.

The slope of the segment $[P_1,P_2]$ is

$$\alpha = \tan^{-1}\left(\frac{\sin\alpha_3 - \sin\alpha_1}{\cos\alpha_3 - \cos\alpha_1}\right) \tag{7}$$

Chip flow angle is then deduced from relation .

CFD predicted by the Analytical Wang and Mathew Model

The model of Wang and Mathew (1995) is based on some assumptions suggested by Young et al. (1987). The main assumption is that only friction force acting at the tool-rake face has an effect on the CFD. In the model, the chip is considered as a series of infinitesimal elements. As shown in Figure 6, each element has its thickness and orientation. The friction force was assumed linearly proportional to the undeformed chip thickness and the direction for each element coincided with the local chip velocity. Based on these assumptions, the magnitude of the friction force dF_0, shown in Figure 6, acting on the arbitrary small chip element can be expressed by the relation

$$dF_0 = udA = ut(s)\,ds \tag{8}$$

Where u is the friction force intensity, dA is the area of the small chip element, ds is the width of the element, and $t(s)$ is the varying undeformed chip thickness in the rake face plane. dF_0 can be decomposed on two components in the reference defined in Figure 6:

$$\mathrm{df}_{ox} = dF_o \sin\Omega_o \tag{9}$$
$$\mathrm{dF}_{oy} = dF_o \cos\Omega_o$$

Where Ω_0 is the angle made by dF_0 with the positive Y axis and given by

$$\Omega_o = \pi/2\text{-}\theta \tag{10}$$

where θ is the angle made between the positive X axis and the direction of elementary friction force. Expressing Eq. in an integral form gives

$$F_{ox} = u\int \sin\Omega_o dA$$
$$F_{oy} = u\int \cos\Omega_o dA \tag{11}$$

As the chip velocity is assumed to be coincident with the friction force vector, the angle made by the resultant friction force F_0 and the positive Y axis can be found from

$$\overline{\Omega}_o = \tan^{-1}\left[\frac{F_{ox}}{F_{oy}}\right] = \tan^{-1}\left[\frac{\int \sin\Omega_o dA}{\int \cos\Omega_o dA}\right] \tag{12}$$

Since friction force intensity u is eliminated in the above equation, the evaluation of $\overline{\Omega}_o$ can be made from the tool and cut geometry only.

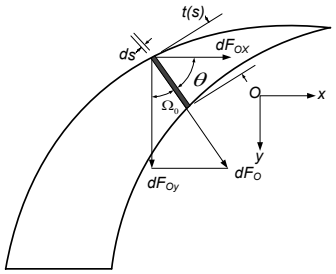

Figure 6: Model for predicting chip flow angle caused by nose radius cutting edge.

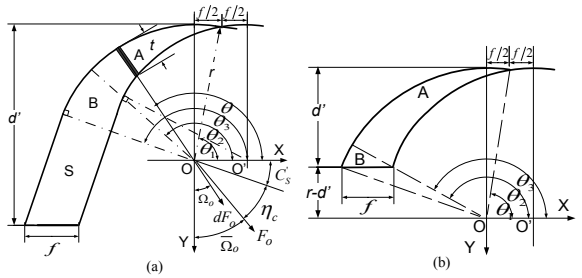

Figure 7: Geometrical conditions of chip flow for a nose radius insert, (a) Case 1: engaged side and nose radius edges and (b) Case 2: engaged nose radius edge.

The chip flow angle η_c, which is measured from the normal to the straight major cutting edge of the tool in the rake face plane, is deduced from

$$\eta_c = \pi/2 - C_s^{'} - \overline{\Omega}_o \tag{13}$$

As reported in Wang and Mathew (1995), four configurations can be defined to evaluate the CFD. Two cases are treated in Figure 7, which include all undeformed chip areas obtained with cutting conditions of Table 1 and Table 2, used in experiments.

Case 1: engaged side cutting and nose radius edges: in this case $d > k_s r$ and $f \le k_e r$, where

$$k_s = \cos i\cos C_e \cot C_s^{'} + \left(1-\csc C_s^{'}\right)\cos i \sec C_s^{'}$$
$$\left[\left(\tan\alpha_n \tan C_s + \sin i\right)^2 + \cos^2 i \sec^2 C_s\right]^{-1/2} \tag{14}$$

with $k_s = \cos i$ for particular case C_s=0. While

$$k_e = 2\sin C_e \cos i \sec\left(C_e - C_s\right)$$
$$\left[\left\{\tan\alpha_n + \tan\left(C_e - C_s\right)\sin i\right\}^2 + \cos^2 i \sec^2\left(C_e - C_s\right)\right]^{-1/2} \tag{15}$$

and $C_s^{'}$ is found from equation

$$C_s^{'} = \cos^{-1}\left[\frac{1+\sin i \tan C_s \tan\alpha_n}{\left[\left(\tan\alpha_n \tan C_s + \sin i\right)^2 + \cos^2 i \sec^2 C_s\right]^{1/2}}\right] \tag{16}$$

To integrate Eq., undeformed chip area is decomposed into three regions, as shown in Figure 7. Regions A and B correspond to the nose radius edge and S to the straight part of the major cutting edge. In regions A and B, the undeformed chip thickness is given by the two following equations, respectively

$$t_A(\theta) = r - f\cos\theta - \left(r^2 - f^2\sin^2\theta\right)^{1/2}$$
$$t_B(\theta) = r - \left(f\cos C_s^{'} - r\right)\sec\left(\theta - C_s^{'}\right) \tag{17}$$

where $\theta_1 \le \theta \le \theta_2$ for region A, and $\theta_2 \le \theta \le \theta_3$ for region B.

The limit angles are $\theta_1 = \cos^{-1}(f/2r)$, $\theta_2 = \pi/2 - \tan^{-1}\left[\left(r\sin C_s'\right)/\left(r\cos C_s' - f\right)\right]$ and $\theta_3 = \pi - C_s'$.

Note that θ is measured counter-clockwise form the positive X axis to the elemental chip. So, in both regions A and B, the angle Ω_0 in Eq. is given by

$$\Omega o\,(\theta) = \theta - \pi/2 \tag{18}$$

For region S, the small thickness segments, which have the same orientation with the corresponding friction force components, act in the same direction in their respective region. Thus, the orientation angle Ω_{0s} for region S can be found from

$$\Omega_{os} = \pi/2 - C_s' \tag{19}$$

Factors containing Ω_0 can be taken out from the integrals when evaluating Eq. for region S. The area of this region can be determined from the associated cut geometry and given by

$$A_S = f\left[d' - r\left(1 - \sin C_s'\right) - 1/4\, f \sin\left(2C_s'\right)\right] \tag{20}$$

where d' is the projection of depth of cut, d, in the rake face:

$$d' = d\cos C_s \sec i\left[\left(\tan\alpha_n \tan C_s + \sin i\right)^2 + \cos^2 i \sec^2 C_s\right]^{1/2} \tag{21}$$

The integral in Eq. are taken over the entire area of the undeformed chip section. Taking into account the relationship $dA = t(\theta)\, ds \approx t(\theta)\, r d\theta$ for regions A and B, Eq. can be expressed as

$$\overline{\Omega}_o = \tan^{-1}\left[\frac{\int_{\theta_1}^{\theta_2}\cos(\theta)t_A(\theta)rd\theta + \int_{\theta_2}^{\theta_3}\cos(\theta)t_B(\theta)rd\theta + A_S\cos C_s'}{\int_{\theta_1}^{\theta_2}\sin(\theta)t_A(\theta)rd\theta + \int_{\theta_2}^{\theta_3}\sin(\theta)t_B(\theta)rd\theta + A_S\sin C_s'}\right] \tag{22}$$

Case 2: engaged nose radius edge: $d \le k_s r$ and $f \le k_e r$

In this case $\overline{\Omega}_o$ is evaluated by only considering regions A and B, thus:

$$\overline{\Omega}_o = \tan^{-1}\left[\frac{\int_{\theta_1}^{\theta_2}\cos(\theta)t_A(\theta)rd\theta + \int_{\theta_2}^{\theta_3}\cos(\theta)t_B(\theta)rd\theta}{\int_{\theta_1}^{\theta_2}\sin(\theta)t_A(\theta)rd\theta + \int_{\theta_2}^{\theta_3}\sin(\theta)t_B(\theta)rd\theta}\right] \tag{23}$$

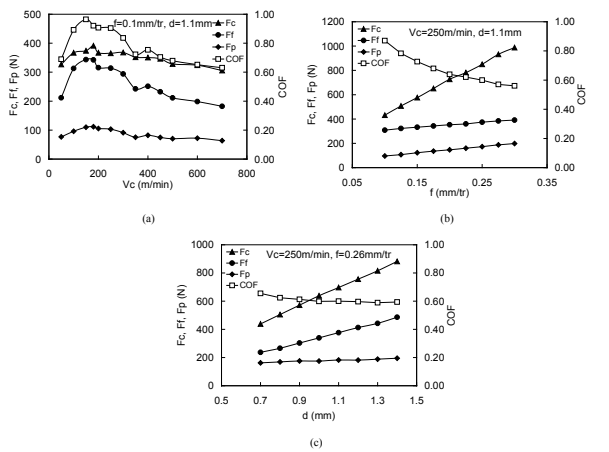

Figure 8: Measured average cutting force components and apparent coefficient of friction in the case of turning with flatted insert.

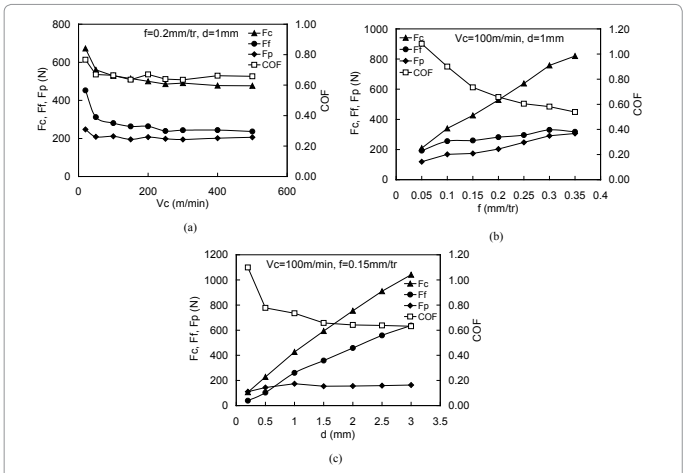

Figure 9: Measured average cutting force components and apparent coefficient of friction in the case of turning with grooved insert.

The evaluation of Eq. or can be performed analytically, as done by Wang and Mathew (1995). In the present study, numerical integration, using adaptive Simpson's rule, is performed in MATLAB® software. Knowing $\overline{\Omega}_o$, the CFD in the cutting plane is then deduced from the relationship .

Results and Discussion

Analysis of measured cutting force components

The evolution of measured cutting force components (F_c, F_f *and* F_p) with respect to cutting parameters (V_c, f, and d), are reported in Figure 8 for the case of turning with flatted uncoated inserts and Figure 9 for the case of turning with grooved coated inserts. The coefficient of friction (COF), defined as the ratio of tangential force by the normal force on the rake face (i.e. $COF = \sqrt{F_f^2 + F_p^2}/F_c$ in considered cases) is also plotted. For almost cutting conditions $F_c > F_f > F_p$. The performed tests show that workmaterials exhibit different sensitivity of cutting force components to the cutting speed.

For machining the AISI 1045 steel with flatted uncoated insert, as shown in Figure 8(a), up to about 200 m/min cutting force components increase and beyond decrease. This is due to the increase of the COF at low cutting speed, as shown in Figure 8(a). The COF increases because cutting inserts are uncoated and sliding velocity at the tool-chip interface, which is proportional to the cutting speed, is not high enough to promote sliding. As reported in Kagnaya (2009) a built-up -edge effect with adhesion of the workmaterial on the rake face of inserts is observed in this range, sign that sticking by sliding area ratio is higher, while beyond about 200 m/min the sliding is more promoted. In addition, at higher cutting speed the softening effect due to heat generated by plastic deformation in removed layer of the workmaterial, which results in temperature raise in the cutting zone, has an impact on the decease of the flow stress of the workmaterial, and therefore on cutting force components. The increase of the feed rate and depth of cut, as shown in Figure 8(b) and (c) Figure 8(c) respectively, results in the increase of all cutting force components . Their evolution is quasi linear. In the same time the COF decreases nonlinearly.

In the other hand, this is not the case when machining the AISI 304L steel with grooved coated inserts, as shown in Figure 9(a), where cutting force components decreases rapidly with the increase of the cutting speed up to 100 m/min, and tends to stagnate beyond.

Observations of cutting inserts did not reveal any apparent adhesion of the workmaterial on the rake face of inserts. The COF, as shown in Figure 9(a), follows the same evolution tendency with respect to the cutting speed evolution. The increase of the feed rate and depth of cut, as shown in Figure 9 (b) and (c) Figure 9 (c) respectively, results in the increase of all cutting force components . Their evolution is quasi linear. In the same time the COF decreases nonlinearly.

Analysis of the chip flow direction

To analyse the CFD in turning with flatted and grooved inserts, measured cutting force components F_f and F_p, reported in Figure 8 and Figure 9, are used to estimate the experimental value of the CFD with Eq. , considered as reference value. The described Colwell and Wang and Mathew models, described in Section 3.2 and Section 3.3 respectively, are then used to predict the CFD. Comparison between predicted and experimental CFD in cases of using flatted and grooved inserts are given in **Fi**gure 10 and Figure 11, respectively. A global overview of these figures shows that experimental chip flow angles are close to the predicted values with the two models. In all cases, Wang and Mathew model gives lower values of the chip flow angle, while Colwell model gives higher values. The Colwell model and Wang and Mathew model can be considered, respectively, as a lower and upper bounds models.

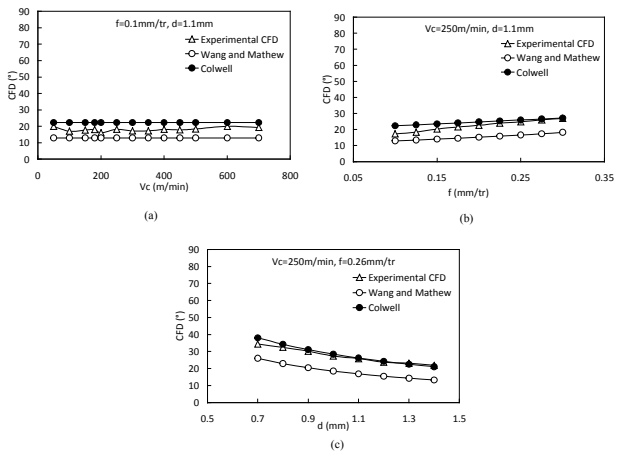

Figure 10: Comparison between predicted and experimental CFD in the case of turning with flatted uncoated inserts.

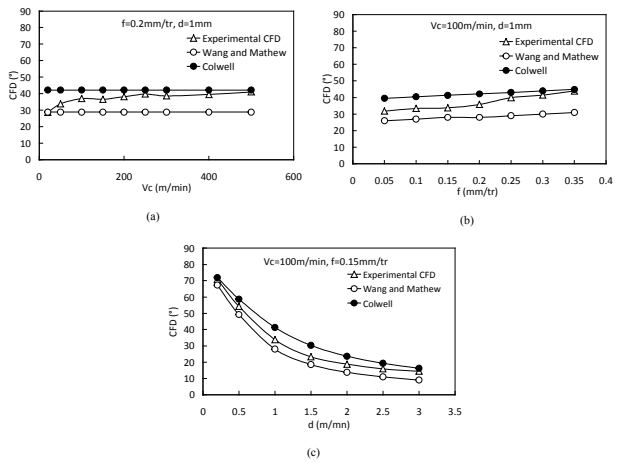

Figure 11: Comparison between predicted and experimental CFD in the case of turning with grooved coated inserts.A

For turning tests with flatted inserts, the experimental CFD is slightly sensitive to cutting speed (Figure 10(a)). The average value of the chip flow angle is about 18°, which is between 13° obtained with the Colwell model and 22° obtained with the Wang and Mathew model. It can be noted that these models are a velocity independent; experimental values of the CFD confirm the model assumptions in case of flatted rake face. At high cutting speed (Figure 10(a)), the experimental CFD is close to the Colwell's CFD. The effect of feed rate in the range of 0.1 to 0.3 mm/tr, for fixed cutting speed (250 m/min) and depth of cut (1.1 mm), is shown in Figure 10(b). Increasing the feed rate increases slightly the chip flow angle in the browsed range. The experimental flow angle tends to that predicted by the Colwell model. The chip flow angle gap in the range 0.1 to 0.3 mm/tr is about 9.7° (experimental), 5.3° (Colwell) and 4.8 (Wang and Mathew). The effect of depth of cut in the tested range 0.7 to 1.4 mm, for fixed cutting speed (250 m/min) and feed rate (0.26 mm/tr), is shown in Figure 10(c). The chip flow angle decreases when increasing the depth of cut, and experimental chip flow angles are very close to that predicted by the Colwell model over the tested range, especially for high depth of cut values.

For turning tests with grooved inserts, as shown in Figure 11, it can be concluded that although the two models ignore the cutting face geometry, however globally same tendencies are observed as for turning tests with flatted inserts. When varying the cutting speed, as shown in Figure 11(a), for fixed feed rate (0.2 tr/m) and depth of cut (1 mm), the experimental CFD evolves as power with saturation law curve, with tendency to stagnate at high cutting speed. The experimental chip flow angle at low cutting speed is close to the one predicted by the Wang and Mathew model, and with increasing cutting speed it tends to the predicted one by the Colwell model. Such evolution tendency was also observed by Zorev (1966), who proposed an empirical power law as function of inclination angle and cutting speed ($\eta_c = iV_c^{-0.08}$). The effect of feed rate on the CFD in the range of 0.05 to 0 .35 mm/tr, for fixed cutting speed (100 m/min) and depth of cut (1 mm), is shown in Figure 11(b). The experimental chip flow angle gap is about 12°. This effect is less pronounced compared to the effect of depth of cut (Figure 11(c)), since the feed rate modifies slightly the engaged part of the nose radius edge, and the engaged part of the side cutting edge remains the same when depth of cut is fixed. For low feeds, the experimental chip flow angle is slightly close to the predicted one by the Wang and Mathew model, while for high feeds it tends to the predicted values by the Colwell model. When varying the depth of cut over a large range (0.2 to 3 mm), the CFD strongly varies from 70° to 15°, as shown in Figure 11(c). In the first half range (from 0.2 to 1.5 mm), the chip flow angle decreases drastically from 70° to 23° (gap of 47°), while in the second half range (from 1.5 to 3 mm), the chip flow angle decreases slightly from 23° to 14° (gap of 9°). Indeed, for small depths of cut the effect of nose radius on the CFD is very pronounced, since elemental engaged cutting edges of the nose radius edge act in different directions and this part of the engaged cutting edge is the higher. While for high depths of cut the CFD tends to stagnate, since the effect of engaged side cutting edge tends to predominate, and elemental edges in this part act in the same direction. Experimental chip flow angles are close to that predicted by the Colwell model for the highest values of depth of cut.

Globally, predicted chip flow angles are in the order of the experimental ones. The tool rake face geometry of the grooved insert has a low impact on the CFD under used cutting conditions, since the two adopted models did not take into account the rake face geometry and predicts well the CFD. It is important to note assumption that the experimental CFD corresponds to the direction of the friction force on the rake face is relatively true. As reported by Yegneswaran (2001),

using CCD camera for the CFD measurement and dynamometer system for the friction force measurement, these two directions may differ slightly under same cutting conditions. This may also have an impact on the difference between the real CFD and the determined one from measured cutting force components. However, this is coherent with the main assumption of the Wang and Mathew model that assumes the CFD collinear with the resultant of elemental frictional forces. Finally it can be noted that the workmaterial has no effect on the CFD, since although different materials are machined, the two models, which are workmaterial independent, predict well the CFD with upper and lower bounds.

Conclusions

Experimental and theoretical analysis of the chip flow direction in turning process using flatted and grooved inserts has been performed in this study. From the experimental CFD, assessed with measured cutting force components, based on assumption that CFD is collinear with the frictional force on the rake face, it has been shown that the CFD is little sensitive to the cutting speed in the two cases. However, for turning tests with grooved insert tendency to stabilisation of CFD is observed at high cutting speed. It has been shown that the CFD is highly sensitive to the depth of cut, followed, by the feed rate and then much lower by the cutting speed. The strong effect of the depth of cut on the CFD is due to the fact that the effect of the nose radius on CFD is predominant for small depths of cut, since elemental engaged cutting edges of the nose radius edge act in different directions. While for high depths of cut the CFD tends to stagnate, since the effect of the engaged side cutting edge tends to predominate and elemental edges in this part act in the same direction.

It can be concluded that the tool rake face geometry, under used cutting conditions, has a little impact on the CFD, since the two adopted models did not take into account the rake face geometry and predict well the CFD. Using the assumption of flat tool rake face may be sufficient to determine the CFD with acceptable accuracy when machining metallic materials. In this study two different steel materials have been machined (AISI 1045 with flatted inserts and AISI 304L with grooved inserts), since the models are material independent and predict well the CFD, it can be concluded that metallic materials has a little effect on the CFD. Finally, inclination and normal rake angles are considered equal to zero in this study, so as a future work the effect of these angles on the CFD will be investigated when machining with other grooved inserts.

References

1. Jared BH, Dow TA (2001) Investigation of the direction of chip motion in diamond turning, Precision Engineering. J International Societies for Precision Engineering and Nanotechnology 25: 155-164.
2. Stabler GV(1951) The fundamental geometry of cutting tools. Proceedings of the Institution of Mechanical Engineers 165, 14–21.
3. Stabler GV (1964) The chip flow law and its consequences. Advances in Machine Tool Design and Research, Pergamon, Oxford: 243-251.
4. Armarego EJA, Brown RH (1969) The Machining of Metals. Prentice Hall, New Jersey.
5. Colwell LV (1954) Predicting the angle of chip flow for single-point cutting tools. Transactions of ASME 76:199-204.
6. Wang J, Mathew P (1995) Development of a general tool model for turning operations based on a variable flow stress theory. Int J Mach Tools and Manu 35: 71-90.
7. Russell JK, Brown RH (1966) The measurement of chip flow direction. Int J Mach Tool Design Res 6: 129-38.
8. Kronenberg M (1966) Machining science and application. Theory and practice for operation and development of machining processes. Pergamon Press, Oxford.
9. Zorev NN (1966) Metal Cutting Mechanics. Pergamon Press, Oxford.
10. Moufki A, Dudzinski D, Molinari A, Rausch M (2000) Thermoviscoplastic modelling of oblique cutting: forces and chip flow predictions. Int J Mech Sci 42: 1205-1232.
11. Strenkowski JS, Shih AJ, Lin JC (2002) An analytical finite element model for predicting three-dimensional tool forces and chip flow. Int J of Mach Tools and Manu 42: 723-731.
12. Usui E, Hirota A, Masuko M (1978) Analytical predictions of three dimensional cutting process Part 1: Basic cutting model and energy approach. J Eng or Industry 100: 222-228.
13. Usui E, Hirota A (1978) Analytical prediction of three dimensional cutting process Part 2: Chip formation and cutting force with conventional single point tool. J Eng for Industry 100: 229-235.
14. Seethaler RJ, Yellowley I (1997) An upper-bound cutting model for oblique cutting tools with a nose radius. Int J Mach Tools and Manu 37: 119-134.
15. Adibi-Sedeh, AH, Madhavan V, Bahr B (2002) Upper bound analysis of oblique cutting with nose radius tools. Int J Mach Tools and Manu 42: 1081-1094.
16. Zou GP, Yellowley I, Seethaler RJ (2009) A new approach to the modelling of oblique cutting processes. Int J Mac Tools and Manu 49: 701-707.
17. Fang N (1998) An improved model for oblique cutting and its application to chip-control research. J of Mater Process Technol 79: 79-85.
18. Wang J (2001) Development of a chip flow model for turning operations. Int J Mach Tools and Manu 41: 1265-1274.
19. Kishawya HA, Lia L, EL-Wahab AI (2006) Prediction of chip flow direction during machining with self-propelled rotary tools. Int J Mach Tools and Manu 46: 1680-1688.
20. Young HT, Mathew P, Oxley PLB (1987) Allowing for nose radius effects in predicting the chip flow direction and cutting forces in bar turning. Proceedings of the Institution of Mechanical Engineers: Part C 201 (C3): 213-226.
21. Kagnaya T (2009) Contribution to the identification of wear mechanisms of a WC-6% Co in machining and by a tribological and thermal approach.
22. Yegneswaran K (2001) Deviation between the sliding direction of the chip over the tool and the direction of the friction force in oblique cutting.